Protonated Carbonic Acid and the Trihydroxymethyl Radical in the Gas Phase. A Neutralization−Reionization Mass Spectrometric and ab Initio/RRKM Study

Pascal Gerbaux[†] and František Tureček*[,‡]

Organic Chemistry Laboratory, University of Mons-Hainaut, 19 Avenue Maistriau, B-7000 Mons, Belgium, and Department of Chemistry, Bagley Hall, Box 351700, University of Washington, Seattle, Washington 98195-1700

Received: January 17, 2002; In Final Form: April 5, 2002

Gas-phase protonation of carbonic acid is predicted to occur preferentially at the carbonyl oxygen with the 298 K proton affinity that was calculated as PA = 741 and 775 kJ mol^{-1} for the syn- and anti-conformer, respectively. The hydroxyl groups are less basic with a topical PA = 660 kJ mol^{-1}. The standard enthalpy of formation of gas-phase carbonic acid was calculated as $\Delta H^{\circ}_{f,298}$ = −614 kJ mol^{-1}. Collisional neutralization of protonated carbonic acid, anti-**1**$^{+}$, yields transient trihydroxymethyl radicals that dissociate rapidly by loss of a hydrogen atom, so that no survivor species are observed on a 360 ns time scale. High-level ab initio calculations with G2(MP2), G2, B3-MP2, and QCISD(T)/6-311+G(3df,2p) find two stable conformers of trihydroxymethyl radicals, anti-**1** and syn-**1**, that interconvert rapidly by O−H bond rotations. The lowest-energy dissociation of anti-**1** is loss of a hydrogen atom which requires 93 kJ mol^{-1} in the transition state and forms the anti-conformer of carbonic acid with an overall reaction enthalpy, $\Delta H_{rxn,0}$ = 18 kJ mol^{-1}. Four other [C,H_3,O_3] isomers are found by calculations to be local energy minima, e.g., hydrogen-bonded complexes [O═C−O···H···OH_2]$^{\bullet}$ (**2**) and [HO−H···O═C−OH]$^{\bullet}$ (**3**), and dihydroxymethoxy radicals anti-**4** and syn-**4**. Of these, **2** was generated transiently in the gas phase and found to dissociate rapidly to water and CO_2. Kinetic isotope effects on dissociations of anti-**1** and syn-**1** are analyzed by RRKM calculations and used to estimate the radical internal energy, which can be expressed as a simple sum of the cationic precursor internal energy and the energy gained by Franck−Condon effects on collisional electron transfer.

Introduction

Carbonic acid is one of the textbook elusive molecules[1] that has been generated only recently in the gas phase and characterized by mass spectrometry.[2] Protonated forms of carbonic acid have been studied by NMR spectroscopy,[3] and a symmetrical conformer has been postulated to exist in solution. However, the fundamental energy parameters of carbonic acid such as enthalpy of formation, proton affinity, and ionization energy are unknown. Ions corresponding to protonated carbonic acid have been generated in the gas phase[4] and shown by a combination of deuterium and ^{18}O labeling to have the structure of a trihydroxymethyl cation (**1**$^{+}$).

Here we utilize cation **1**$^{+}$ for the generation of trihydroxymethyl radical, $C(OH)_3$ (**1**), which can be viewed as a hydrogen atom adduct to carbonic acid. Our interest in **1** stems from the unusual combination of three π-electron donating groups that interact with the open shell electronic system of the central carbon atom. Methyl radicals bearing π-electron donating (OH, NH_2), π-electron acceptor (CN, NO_2), and σ-electron withdrawing (F, Cl), substituents have been of keen interest to both experimentalists[5] and computational chemists.[6] The popularity of substituted methyl radicals stems in part from the fact that they represent the simplest models for studying the effects of functional groups on the dissociation energies of adjacent C−H and C−C bonds. In addition, hydroxylated and halogenated methyl radicals play an important role in tropospheric oxidations and stratospheric photolysis, respectively.[7] While several substituted methyl radicals have been generated from stable precursors in the gas phase by classical methods such as pyrolysis,[8] photolysis,[9] or H atom abstraction,[10] di- and trisubstituted methyl radicals containing combinations of OH and NH_2 groups are less easily available because of lack of suitable precursors.

For such difficult systems, neutralization−reionization mass spectrometry (NRMS)[11] provides a general synthetic methodology to generate substituted methyl radicals in the gas phase and study their unimolecular properties on the microsecond time scale. NRMS relies on the generation in the rarefied gas phase of a stable cation or anion that has the same bond connectivity as the target radical. The ion precursor is accelerated to a high velocity (typically 100,000−200,000 m/s) and discharged by a glancing collision with a gaseous target. For neutralization of cations, polarizable electron donors such as xenon, trimethylamine, *N*,*N*-dimethylaniline, or dimethyl disulfide are used to achieve efficient electron transfer, while minimizing ion collision-induced dissociations and internal excitation of the incipient radicals. NRMS has been used to generate several transient monosubstituted methyl radicals, e.g., CH_2OH,[12] CH_2Cl,[13] $CH_2N(CH_3)_2$,[14] CH_2NO_2,[15] as well as disubstituted radicals, e.g., FCHOH,[16] CHFCl and $CHCl_2$,[17] $CH(OH)_2$,[18] and $CH(OH)NH_2$.[19]

In this work, we report the first experimental and computational study of **1**. Radical **1**, its isotopomers $C(OH)_2(OD)$ (**1a**), $C(OH)(OD)_2$ (**1b**), and $C(OD)_3$ (**1c**), and a hydrogen-bonded complex, O═C−O···H···OH_2 (**2**) are generated unambiguously from stable cation precursors and characterized by NRMS. We

* Corresponding author. Tel.: (206) 685-2041. Fax: (206) 685-3478. E-mail: turecek@chem.washington.edu.
† University of Mons-Hainaut.
‡ University of Washington.

10.1021/jp020162c CCC: $22.00
Published on Web 05/29/2002

wish to show that **1** is an intrinsically stable species that is made highly reactive by large Franck−Condon effects on collisional electron transfer that largely determine the radical unimolecular chemistry in the gas phase. We also report the enthalpy of formation, proton affinity, adiabatic, and vertical ionization energies of carbonic acid conformers that were obtained at high levels of ab initio theory.

Experimental Section

Materials. Dipropyl carbonate (**5**) (Aldrich), dihydroxyfumaric acid (**6**) (Aldrich), and dimethyl disulfide (DMDS, Aldrich) were used as received. (Ethyl-d_5)-propyl-carbonate (**7**), ethyl-(propyl-d_7)-carbonate (**8**), di-(ethyl-d_5)-carbonate (**9**), (ethyl-d_5)-butyl ether (**10**) were prepared by standard procedures as follows.

(Ethyl-d_5)-propyl-carbonate (**7**). A mixture of propyl chloroformate (0.02 mol, Aldrich), ethanol-d_6 (0.02 mol, Aldrich), and pyridine (0.025 mol, Aldrich) in 40 mL of methylene chloride was stirred at room temperature for 5 h. The dichloromethane solution was washed with 20 mL of 1 M HCl, 20 mL of water, the solvent was evaporated in vacuo, and the crude product was distilled at atmospheric pressure (bp 133−135 °C).[20]

Ethyl-(propyl-d_7)-carbonate (**8**). A mixture of ethyl chloroformate (0.02 mol, Aldrich), propanol-d_8 (0.02 mol, Aldrich), and pyridine (0.025 mol) was stirred in 40 mL of methylene chloride at room temperature for 5 h. The solution was worked up as for compound **7** and the product was distilled at atmospheric pressure (bp 148−150 °C).[20]

Di-(ethyl-d_5)-carbonate (**9**). To a solution of ethanol-d_6 (0.02 mol, Aldrich) and triphosgene (0.0072 mol, Aldrich) in 40 mL of methylene chloride was added pyridine (0.025 mol) dropwise at room temperature. The resulting mixture was stirred for 30 min and another portion of 0.02 mol of ethanol-d_6 was added, followed by 0.025 mol of pyridine. After the reaction mixture was stirred for 2 h, it was quenched by adding 20 mL of 1 M HCl and 20 mL of water. The organic phase was separated, dried with magnesium sulfate, the solvent was evaporated in vacuo, and the crude product distilled at atmospheric pressure (bp 126−128 °C).[21]

(Ethyl-d_5)butyl ether (**10**). 1-Iodobutane (0.05 mol, Aldrich), ethanol-d_6 (0.05 mol), and freshly prepared silver oxide (0.05 mol) were stirred overnight in methylene chloride (20 mL). The product was distilled off directly from the reaction mixture and the fraction boiling at 93−95 °C was collected.

Methods. Spectra were taken on the University of Washington tandem quadrupole acceleration−deceleration mass spectrometer described previously,[22] hereinafter denoted as UW, and the University of Mons-Hainaut six-sector tandem mass spectrometer,[23] denoted as UMH. In the UW measurements, cations were generated in a standard electron ionization (EI) source. Typical ionization conditions were as follows: electron energy 70 eV, emission current 500 μA, and source temperature 200 °C. Stable precursor cations were passed through a quadrupole mass filter operated in the radio frequency-only mode, accelerated to a total kinetic energy of 8250 eV, and neutralized in the collision cell floated at −8170 V. Dimethyl disulfide (DMDS) or ammonia (NH_3) were introduced to the differentially pumped collision cell at a pressure such as to achieve 70% transmittance of the precursor ion beam. The ions and neutrals were allowed to drift to a four-segment conduit,[11c] where the ions were reflected by the first segment floated at +250 V. The neutral flight times for the $C(OH)_3$ radicals in standard NRMS measurements were 3.8 μs. The fast neutral species were reionized in the second collision cell with oxygen at a pressure such as to achieve 70% transmission of the precursor ion beam. The ions formed in the second collision cell were decelerated, the fast neutrals were blocked by a chicane lens that also provided an ion kinetic energy filter, and the ions passing the filter were analyzed by a second quadrupole mass filter operated at unit mass resolution. The instrument was tuned daily to maximize the ion current of reionized $CS_2^{\bullet+}$. Typical spectra consisted of 50 accumulated repetitive scans. Variable-time measurements were performed as described previously.[24] The flight times of the neutral intermediates that were used to evaluate the unimolecular dissociation kinetics were 0.36, 1.07, and 1.77 μs.

The UMH measurements were performed on a Micromass large scale tandem mass spectrometer of $c_1E_1B_1c_2E_2c_3c_4E_3B_2c_5E_4$ geometry (E stands for electric sector, B for magnetic sector and c for collision cell).[23] Typical conditions were 8 kV accelerating voltage, 200 μA electron trap current (in the electron ionization mode, EI), 1 mA (in the chemical ionization mode, CI), 70 eV ionizing electron energy, and 200 °C ion source temperature. Solid samples were introduced with a direct insertion probe, while liquid samples were injected in the ion source via a heated (180 °C) septum inlet. Collision-induced dissociation (CID) with O_2 of mass selected ions of 8 keV kinetic energy was performed in c_4 and the CID spectra were recorded by scanning E_3 and collecting the ions in the fifth field-free region with an off-axis photomultiplier detector. Dissociations of mass-selected metastable ions occurring in the third field-free region were monitored with the first off-axis detector after scanning the second electric sector (mass-analyzed ion kinetic energy spectra, MIKES). In the NRMS experiments, 8 keV ions were neutralized in c_3 with ammonia at 70% beam transmission and the residual ions were eliminated by floating the intermediate calibration ion source inserted between both cells at 9 keV. Fast neutral species were reionized in c_4 with O_2 at 70% transmission. All spectra were recorded by scanning E_3 and collecting the ions in the fifth field-free region with an off-axis photomultiplier detector.

Calculations. Standard ab initio calculations were performed using the Gaussian 98 suite of programs.[25] Optimized geometries were obtained by density functional theory calculations using Becke's hybrid functional (B3LYP)[26] and the 6-31+G(d,p) basis set. For comparison, an additional set of optimized geometries was obtained by perturbational Moller−Plesset calculations,[27] with excitations of all electrons, MP2(FULL), and the 6-31+G-(d,p) basis set. The B3LYP and MP2 geometries were very similar and yielded single-point G2(MP2) energies that were within 0.3 millihartree (0.8 kJ mol^{-1}). Spin unrestricted calculations were performed for all open-shell systems. Contamination by higher spin states was low in the UHF and UMP2 calculations, and was corrected by spin projection[28] that lowered the total energies by ≤2 millihartree for local minima and ≤5 millihartree for transition states. Stationary points were characterized by harmonic frequency calculations with B3LYP/6-31+G(d,p) as local minima (all real frequencies) and first-order saddle points (one imaginary frequency). The calculated frequencies were scaled with 0.963[29] and used to obtain zero-point energy corrections, enthalpies, entropies, and RRKM rate constants. Improved energies were obtained by single-point calculations at four levels of theory. Composite G2(MP2)[30] and G2[31] energies were obtained from quadratic configuration interaction calculations with single, double, and perturbational triple excitations, QCISD(T)[32] with the 6-311G(d,p) basis set, and basis set expansions from 6-311G(d,p) through 6-311+G-

SCHEME 1

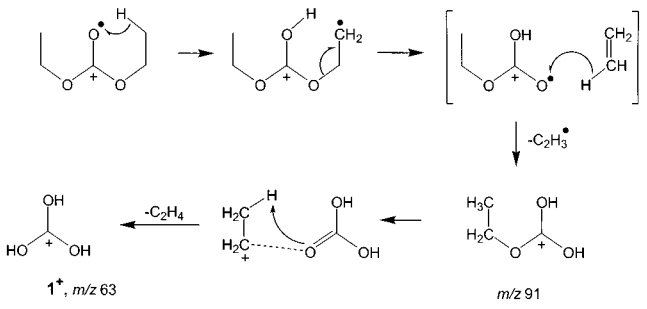

(3df,2p) via perturbational Moller−Plesset calculations, MP2, and MP4(SDTQ). Since we mostly dealt with isogyric reactions in which the number of valence electrons is conserved, empirical corrections for the number of valence electrons[30] were not used. Single-point QCISD(T) calculations were also carried out with the full 6-311+G(3df,2p) basis set. This was motivated by the failure of the G2 scheme to correctly treat CO_2,[33] which appears in several reactions relevant to the system under study. For most of our ions, molecules excluding CO_2, and radicals, the full QCISD(T)/6-311+G(3df,2p) energies were bracketed by those from the composite calculations, with effective energies from the G2 scheme being on average 1.6 millihartree (4.1 kJ mol^{-1}) lower, while those from the G2(MP2) scheme being on average 4.3 millihartree (11.3 kJ mol^{-1}) higher. For selected systems, total energies were also obtained with coupled-cluster calculations[34] with single, double, and uncoupled triple excitations of valence electrons, CCSD(T),[35] using Dunning's correlation-consistent basis set of triple-ζ quality with polarization and diffuse functions on all atoms, aug-cc-pVTZ.[36] Energies from these high-level calculations are compared to composite B3-MP2 energies that were performed with the 6-311+G(3df,2p) basis set, as described previously.[37]

Geometry optimizations of excited electronic states were carried out by spin-unrestricted configuration interaction singles (UCIS)[38] calculations using the 6-31+G(d,p) basis set. Improved excited-state energies were obtained by time-dependent density functional theory calculations[39] using the B3LYP functional and the 6-311+G(3df,2p) basis set.

RRKM calculations were performed using Hase's program[40] that was recompiled and run under Windows NT.[41] Direct count of quantum states was used in 2 kJ mol^{-1} steps from the transition state energy up to 200 kJ mol^{-1} above it. Rotational states were treated adiabatically. The calculated microscopic rate constants, $k(E,J,K)$, were Boltzmann averaged over the rotational states at 473 K, corresponding to the ion source temperature that defines the precursor ion rotational temperature, to give microcanonical rate constants $k(E)$.

Results and Discussion

Specific generation of transient neutral species by NRMS relies entirely upon the knowledge of structures of the ionic precursors. The chemistry of $C(OH)_3^+$, its isotopomers, the $CO_2\cdots H_3O^+$ complex, and their dissociation products are therefore briefly discussed first.

Preparation of $C(OH)_{3-n}(OD)_n^+$ Cations ($n = 0-3$). Cation $\mathbf{1}^+$ can be generated by dissociative ionization of dialkyl carbonates that give the corresponding m/z 63 peak in the electron ionization mass spectra.[42] The first step, loss of $C_2H_3^\bullet$, proceeds by a double hydrogen atom transfer, which is followed by elimination of C_2H_4 that also involves a hydrogen rearrangement. The postulated elimination mechanisms are shown in Scheme 1. The consecutive elimination of a vinyl radical and an alkene is supported by the appearance of intense peaks for metastable ion dissociations.[43]

SCHEME 2

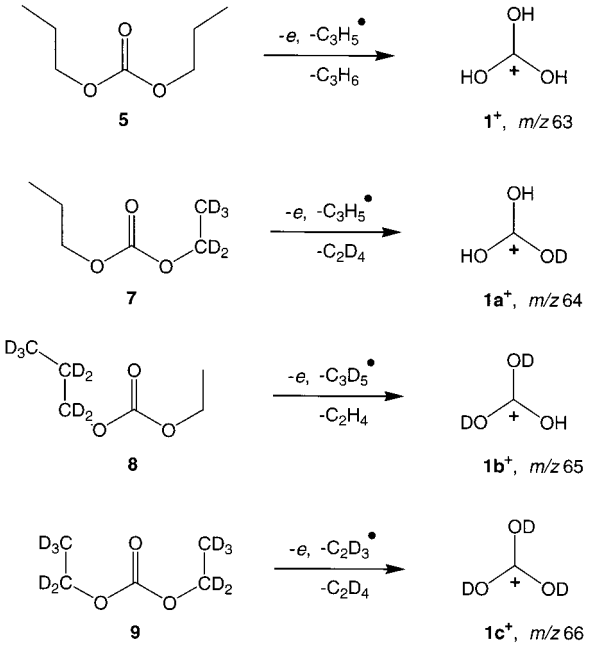

The structure of $C(OH)_3^+$ cations was investigated in detail by Egsgaard and Carlsen who concluded that cation $\mathbf{1}^+$ was the symmetrical trihydroxymethyl species.[4] It was also demonstrated that, starting from an asymmetric dialkyl carbonate precursor, both hydrogen atoms involved in the first step, which is the loss of an alkenyl radical, preferentially originate from the longer alkyl chain.[4] This interesting feature is used in the present work to prepare specifically labeled $C(OH)_{3-n}(OD)_n^+$ ions (Scheme 2). Recently, the isomeric proton-bound ion $[H_2O\cdots H\cdots OCO]^+$ ($\mathbf{2}^+$) was shown to arise by dissociative ionization of dihydroxyfumaric acid.[44] Ion $\mathbf{2}^+$ was easily identified by comparison of its CID spectrum with that of $\mathbf{1}^+$.

We used di-*n*-propyl carbonate as a suitable precursor for the production of pure $\mathbf{1}^+$ (Scheme 2). High-resolution mass spectra (HRMS) confirm the absence of any isobaric interference at m/z 63. The labeled ions, $C(OH)_2(OD)^+$ ($\mathbf{1a}^+$, m/z 64), $C(OH)(OD)_2^+$ ($\mathbf{1b}^+$, m/z 65), and $C(OD)_3^+$ ($\mathbf{1c}^+$, m/z 66), were produced, respectively, from (ethyl-d_5)-propyl-carbonate (**7**), ethyl-(propyl-d_7)-carbonate (**8**), and di-(ethyl-d_5)-carbonate (**9**), but were accompanied by isobaric ions, e.g., $CD_3CD_2OCH_2^+$, $CD_3CD_2OCHD^+$, and $CD_3CD_2OCD_2^+$, respectively (Scheme 2). These isobaric interferences were separated by adjusting the mass resolution to $M/\Delta M \geq 1000$ which allowed unambiguous precursor ion selection.

Ion Dissociations. The metastable and collision-induced dissociations of $C(OH)_{3-n}(OD)_n^+$ cations ($n = 1-3$) were studied under conditions of high mass resolution when mass-selecting the precursor ions. The only observable dissociation of metastable $\mathbf{1}^+$ is elimination of water yielding m/z 45 ions, most likely protonated carbon dioxide, HO−C=O$^+$. This metastable dissociation is associated with a kinetic energy release of $T_{0.5} = 96$ meV. The CID spectrum of $\mathbf{1}^+$ obtained at 8 keV (Figure 1a) showed mainly a loss of a hydrogen atom, yielding ionized carbonic acid at m/z 62, elimination of water giving $COOH^+$ at m/z 45, and formation of $CO_2H_2^{\bullet+}$, $CO_2^{\bullet+}$, HCO^+, $CO^{\bullet+}$, $H_2O^{\bullet+}$, and OH^+ at m/z 46, 44, 29, 28, 18 and 17, respectively. Doubly charged $\mathbf{1}^{2+}$ ions at m/z 31.5 are also formed upon CID with oxygen. The CID spectra of $\mathbf{1a}^+-\mathbf{1c}^+$

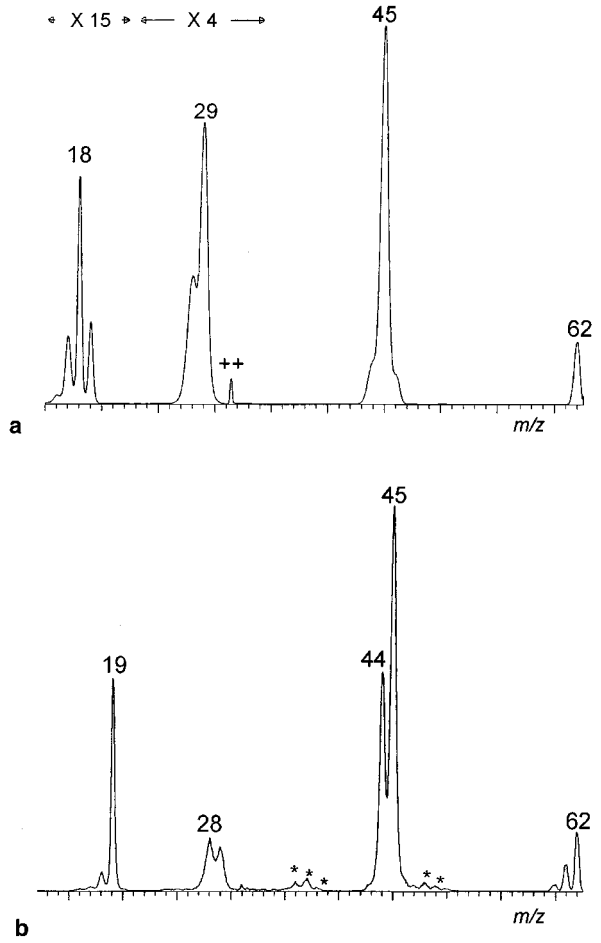

Figure 1. Collision-induced dissociation spectra (O_2, 70%T) of $CH_3O_3^+$ cations (*m*/*z* 63) prepared by dissociative ionization of (a) di-*n*-propyl carbonate, and (b) dihydroxyfumaric acid. Asterisks indicate the peaks originating from a minor $C_5H_3^+$ impurity.

confirm the previous assignments through the corresponding mass shifts to higher mass-to-charge ratios when compared to the unlabeled species (Figure 2a−c). In addition, the CID spectra showed a weak peak at *m*/*z* 19 (or *m*/*z* 22 for **1c**$^+$), corresponding to protonated water, which may be formed from an isomeric species, $[H_2O\cdots H\cdots OCO]^+$ (**2**$^+$) present as a minor contaminant in the precursor ion beam or produced as an intermediate upon collisional activation.

An authentic cation of structure **2**$^+$ was generated by dissociative ionization of dihydroxyfumaric acid (**6**).[44] Although the relative intensity of this *m*/*z* 63 peak in the EI spectrum of **6** is very weak (ca. 0.01% of the *m*/*z* 44 base peak), we succeeded in obtaining the CID spectrum that revealed some interesting differences when compared to the CID spectrum of **1**$^+$ (Figure 1b). In particular, the abundant product ions of H_3O^+ at *m*/*z* 19 and the complementary $CO_2^{\bullet+}$ at *m*/*z* 44 are perfectly consistent with the proposed structure of a proton-bound $H_2O\cdots H^+\cdots OCO$ complex for **2**$^+$ and with the calculated energetics of ion dissociations (vide infra).

Ion Structures and Energies. To substantiate the proposed ion structures and dissociation mechanisms, we performed ab initio and density functional theory calculations of the relevant ion species. The optimized structures are presented in Figure 3, complete geometry parameters can be obtained from the corresponding author upon request. Only singlet structures were investigated, as carbocation triplets are likely to be substantially higher in energy.[45] The ion relative and dissociation energies are summarized in Table 1 and visualized in a potential energy

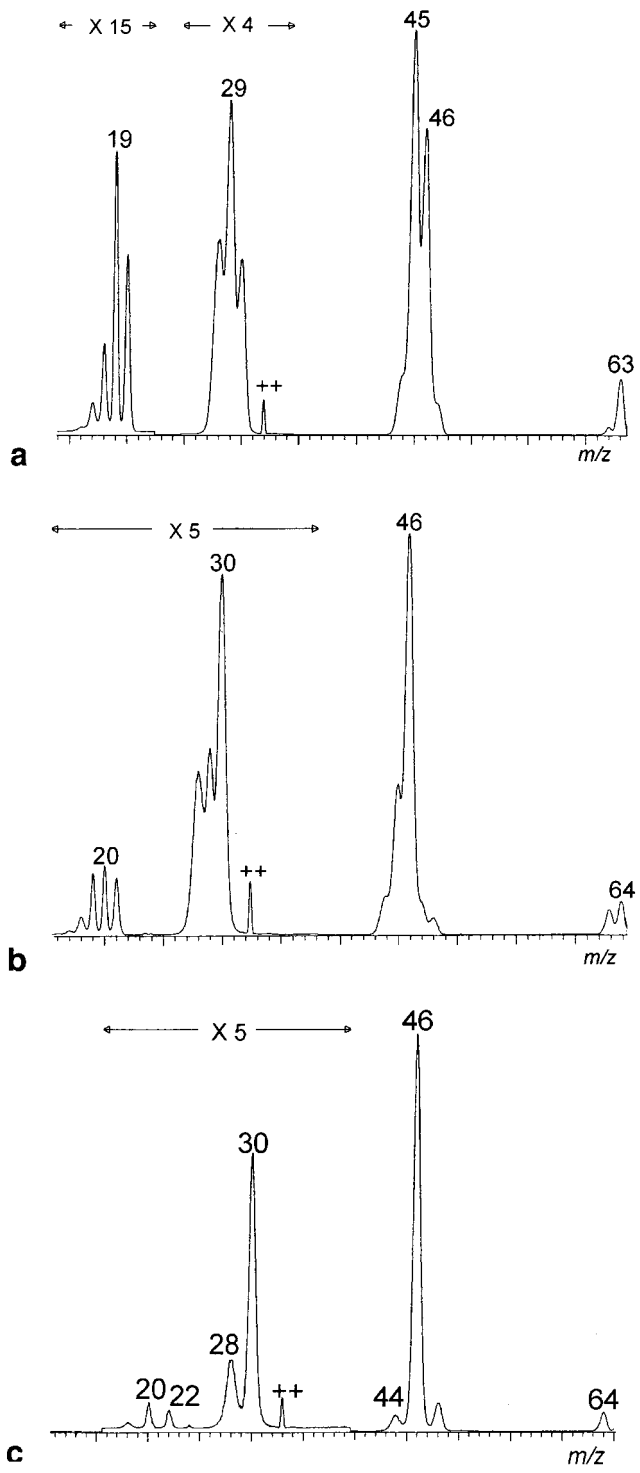

Figure 2. Collision-induced dissociation spectra (O_2, 70%T) of (a) $C(OD)(OH)_2^+$ (**1a**, *m*/*z* 64), (b) $C(OD)_2(OH)^+$ (**1b**, *m*/*z* 65), and (c) $C(OD)_3^+$ (**1c**, *m*/*z* 66).

diagram (Figure 4). The energies presented in the text and Figure 4 are from QCISD(T)/6-311+G(3df,2p) calculations and refer to 0 K, unless stated otherwise. Two conformers (denoted anti-**1**$^+$ and syn-**1**$^+$) of C_{3h} and C_s symmetry, respectively, were found as local energy minima for **1**$^+$. Anti-**1**$^+$ is 25 kJ mol^{-1} more stable than syn-**1**$^+$ and the rotamers are separated by a rotational barrier of 50 kJ mol^{-1} relative to anti-**1**$^+$ (**TS1**, Figure 4). The greater stability of anti-**1**$^+$ follows from the more favorable orientation of the O−H bond dipoles than in syn-**1**$^+$. A third isomer (**11**$^+$) that exists as a local energy minimum can be viewed as an adduct of water and $COOH^+$ (Figure 3).

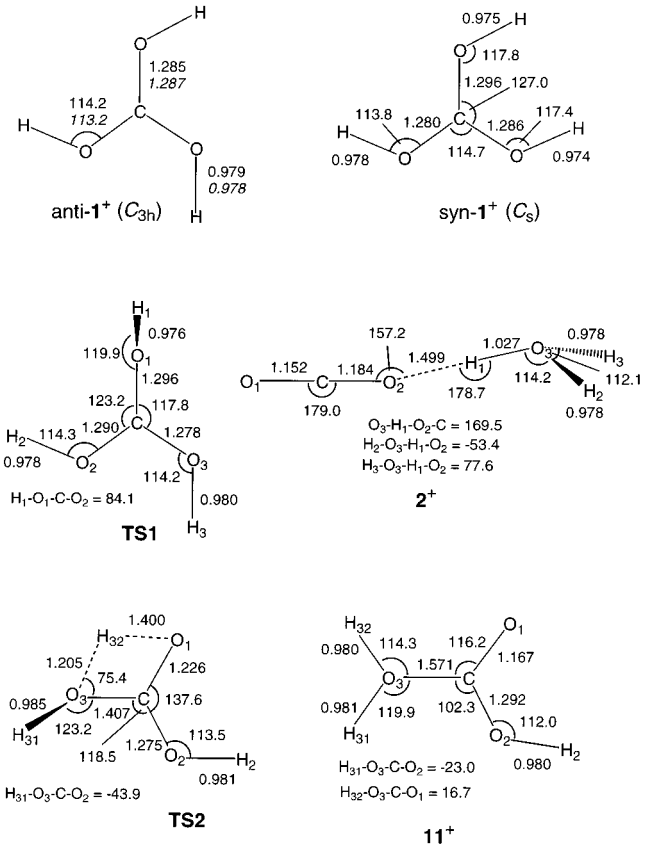

Figure 3. B3LYP/6-31+G(d,p) (roman numerals) and MP2(FULL)/6-31+G(d,p) (italics) optimized structures of $[C,H_3,O_3]^+$ cations. Bond lengths in angstroms, bond and dihedral angles in degrees.

TABLE 1: Ion Relative Energies and Proton Affinities of Carbonic Acid

	relative energy[a]			
species/reaction	G2(MP2)	G2	QCISD(T)[b]	B3-MP2
anti-**1**$^+$	0	0	0	0
syn-**1**$^+$	25	25	25	25
2$^+$	−15	−14	−15	−21
11$^+$	106	106	106	103
TS1 (anti-**1**$^+$→ syn-**1**$^+$)	50	50	50	49
TS2 (anti-**1**$^+$→ **11**$^+$)	218	213	216	214
anti-**1**$^+$ → $COOH^+ + H_2O$	193	188	194	191
syn-**1**$^+$ → syn-**12** + H^+	736	735	736	733
PA(O=C) at 298 K[c]	741	740	741	738
11$^+$ → syn-**12** + H^+	656	655	656	657
PA(OH) at 298 K[d]	660	659	660	660
anti-**1**$^+$ → anti-**12**+ H^+	769	768	769	766
PA at 298 K[c]	775	774	775	772
anti-**1**$^+$ → $CO_2 + H_3O^+$	46	*e*	47	41
syn-**12**$^{+\bullet}$ → $CO_2 + H_2O^{+\bullet}$	96	*e*	97	92
anti-**12**$^{+\bullet}$ → $CO_2 + H_2O^{+\bullet}$	95	*e*		92
syn-**12**$^{+\bullet}$ → $COOH^+ + OH^\bullet$	150	151	150	146
anti-**12**$^{+\bullet}$ → $COOH^+ + OH^\bullet$	150	151		146

[a] In units of kJ mol^{-1} at 0 K unless stated otherwise. [b] From single-point calculations with the 6-311+G(3df,2p) basis set. [c] 298 K topical proton affinities for protonation at the carbonyl oxygen. [d] 298 K topical proton affinity at the hydroxyl group in syn-**12**. [e] G2 calculations fail for CO_2.[33]

At our highest level of theory, ion **11**$^+$ is 106 kJ mol^{-1} less stable than anti-**1**$^+$ (Table 1). Anti-**1**$^+$ and **11**$^+$ are separated by a substantial barrier to hydrogen migration (**TS2**) which is 216 kJ mol^{-1} above anti-**1**$^+$. Dissociation of anti-**1**$^+$ to $COOH^+ + H_2O$ requires 194 kJ mol^{-1} at the thermochemical threshold,

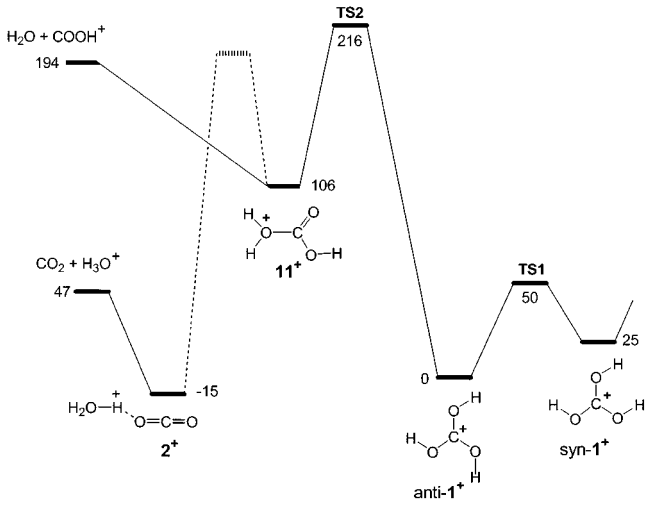

Figure 4. Potential energy diagram for isomerizations and dissociations of $[C,H_3,O_3]$ cations. 0 K energies from single-point QCISD(T)/6-311+G(3df,2p) calculations.

but most likely involves **11**$^+$ as an intermediate. The energy excess in the dissociation, anti-**1**$^+$ → **TS2** → **11**$^+$ → $COOH^+ + H_2O$, $\Delta H_0 = 216-194 = 22$ kJ mol^{-1}, is perfectly consistent with the kinetic energy release in the elimination of water from metastable **1**$^+$ (96 meV = 9.3 kJ mol^{-1}). Considering that the average kinetic energy release, $\langle T \rangle$, is about twice $T_{0.5}$ measured at the metastable peak width at half-maximum ($\langle T \rangle / T_{0.5} = 2.16$ for ideal Gaussian peaks),[46] the metastable ion dissociations suggest that most of the nonfixed ion energy (~20 kJ mol^{-1}) is channeled into the kinetic energy of separating fragments. This indicates that the isomerization, anti-**1**$^+$ → **TS2** → **11**$^+$, is the rate-determining step in the elimination of water from **1**$^+$. This conclusion is important for discussing the role of the ion−molecule complex (**2**$^+$) which is calculated to be the most stable ion isomer, being 15 kJ mol^{-1} more stable than anti-**1**$^+$ (Figure 4). Ion **2**$^+$ shows a tight hydrogen bonding between the bridging H_3O^+ proton and the CO_2 oxygen atom, as illustrated by the corresponding O···H bond distance of 1.50 Å (Figure 3). However, an exothermic isomerization of anti-**1**$^+$ to **2**$^+$ requires at least two hydrogen migrations, which should present a substantial kinetic hindrance.

Enthalpy of Formation of 1$^+$. The calculated enthalpies of dissociations, combined with the reliable experimental enthalpies of formation for H_2O, H_3O^+, CO_2, and $COOH^+$ (ref 42) allow us to obtain the standard enthalpy of formation for anti-**1**$^+$, eq 1 and 2.

$$\text{anti-}\mathbf{1}^+ \rightarrow CO_2 + H_3O^+ \qquad \Delta H_{rxn,298} = 54 \text{ kJ mol}^{-1} \qquad (1)$$

$$\Delta H^\circ_{f,298}(\mathbf{1}^+) = 150 \text{ kJ mol}^{-1}$$

$$\text{anti-}\mathbf{1}^+ \rightarrow COOH^+ + H_2O \qquad \Delta H_{rxn,298} = 203 \text{ kJ mol}^{-1} \qquad (2)$$

$$\Delta H^\circ_{f,298}(\mathbf{1}^+) = 151 \text{ kJ mol}^{-1}$$

The average value from eqs 1 and 2, $\Delta H^\circ_{f,298}$ (**1**$^+$) = 151 kJ mol^{-1}, was further used to assess the energetics of anti-**1**$^+$ formation from di-*n*-alkyl carbonates, as discussed below. It may be noted that the calculated $\Delta H^\circ_{f,298}$ (**1**$^+$) is in good agreement with a previous estimate (155 kJ mol^{-1}) that was based on appearance energy measurements for the formation of **1**$^+$ from diethyl carbonate.[47]

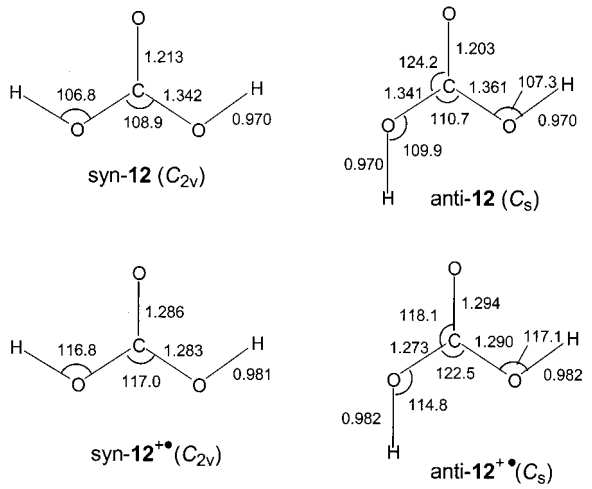

Figure 5. B3LYP/6-31+G(d,p) optimized geometries of carbonic acid neutral and ion conformers.

Generation of Low-Energy 1^+. Because the precursor ion internal energy can affect the stability of the neutral species formed by collisional electron transfer, we also prepared $\mathbf{1}^+$ using charge-exchange with Xe^+ to control the ionization energetics. From the enthalpies of formation of anti-$\mathbf{1}^+$(151 kJ mol^{-1}, vide supra), di-*n*-propyl carbonate (−681 kJ mol^{-1}),[42] propene (20.4 kJ mol^{-1}), and allyl radical (171 kJ mol^{-1}), we calculate the appearance energy for the formation of anti-$\mathbf{1}^+$ as 1023 kJ mol^{-1} or 10.61 eV. Thus, charge-exchange ionization with Xe^+ (RE = 12.13 eV) delivers 12.13 − 10.61 = 1.52 eV to be distributed among the dissociation products roughly in the ratio of their heat capacities, which were calculated as 65, 70, and 64 J mol^{-1} K^{-1} for anti-$\mathbf{1}^+$, propene, and allyl radical, respectively. Upon equipartition of the 1.52 eV excess energy, anti-$\mathbf{1}^+$should be formed with 48 kJ mol^{-1} internal energy. Furthermore, under the high-pressure conditions of CE ionization, the excess internal energy in $\mathbf{1}^+$ is likely to be partially dissipated by collisions with Xe. If fully thermalized, anti-$\mathbf{1}^+$ is calculated to have on average 20 kJ mol^{-1} internal energy at 473 K. Hence, the mean internal energy of $\mathbf{1}^+$ produced by charge-exchange ionization is bracketed between 20 and 48 kJ mol^{-1}.

Structure, Proton Affinity, Ionization Energy, and Enthalpy of Formation of Carbonic Acid. Carbonic acid (**12**) also exists as two conformers, syn-**12** and anti-**12** (Figure 5), which differ in energy by 6.4 kJ mol^{-1} in favor of the syn-rotamer and are separated by a 39 kJ mol^{-1} rotational barrier relative to syn-**12**. From the calculated free energy difference for the rotamers, $\Delta G^\circ_{f,298}$ = 4.5 kJ mol^{-1}, and the symmetry numbers[48] (σ = 2 for syn-**12** and σ = 1 for anti-**12**), one calculates the equilibrium populations as 76% syn-**12** and 24% anti-**12** at 298 K.

Protonation at the carbonyl oxygen in syn-**12** gives syn-$\mathbf{1}^+$ with a proton affinity, PA(syn-**12**) = 741 kJ mol^{-1} (298 K value, Table 1). Protonation at the carbonyl oxygen of the less stable anti-**12** produces the more stable anti-$\mathbf{1}^+$ ion, which makes anti-**12** more basic with PA(anti-**12**) = 775 kJ mol^{-1} at 298 K. The proton affinity of the hydroxyl groups in syn-**12** is substantially lower, PA = 660 kJ mol^{-1}.

The other energy parameters that characterize carbonic acid are the adiabatic ionization energies, for which G2 calculations including corrections for the number of valence electrons give IE_a = 11.29 and 11.23 eV for syn-**12** and anti-**12**, respectively. By comparison, the G2(MP2) and B3-MP2 ionization energies are very similar to the G2 values (Table 2). Interestingly, gas-phase carbonic acid is metastable with respect to dissociation to CO_2 and H_2O which was calculated to be slightly exothermic and have a reaction enthalpy of $\Delta H_{rxn,298}$ = −21.4 kJ mol^{-1} (CCSD(T) value, Table 3). Atomization energies calculated from the G2 and G2(MP2) schemes and the enthalpy of dissociation to CO_2 + H_2O allowed us to estimate the standard enthalpy of formation for gas-phase carbonic acid to fall in the range of $\Delta H^\circ_{f,298}$ = −608 to −623 kJ mol^{-1} (Table 3). At the highest level of theory, which was CCSD(T)/aug-cc-pVTZ in this case, $\Delta H^\circ_{f,298}$ (**12**) = −614 kJ mol^{-1}.

TABLE 2: Ionization and Recombination Energies.

		energy[a]			
species		G2(MP2)[b]	G2[b]	QCISD(T)	B3-MP2
anti-**1**	IE_a	5.82	5.83	5.82	5.84
	IE_v	7.70			7.79
	RE_v	4.06			4.20
syn-**1**	IE_a	5.98	5.99	5.98	6.01
	RE_v	4.13			4.25
2	IE_a	6.11	6.13	6.11	6.11
	RE_v	3.14			3.30
anti-**12**	IE_a	11.22	11.23		11.19
	IE_v	11.66			11.67
syn-**12**	IE_a	11.28	11.29	11.14	11.25
	IE_v	11.74			11.74
COOH	IE_a	7.94	7.96	7.94	7.99

[a] In units of electronvolt. [b] Including empirical corrections for the number of valence electrons.

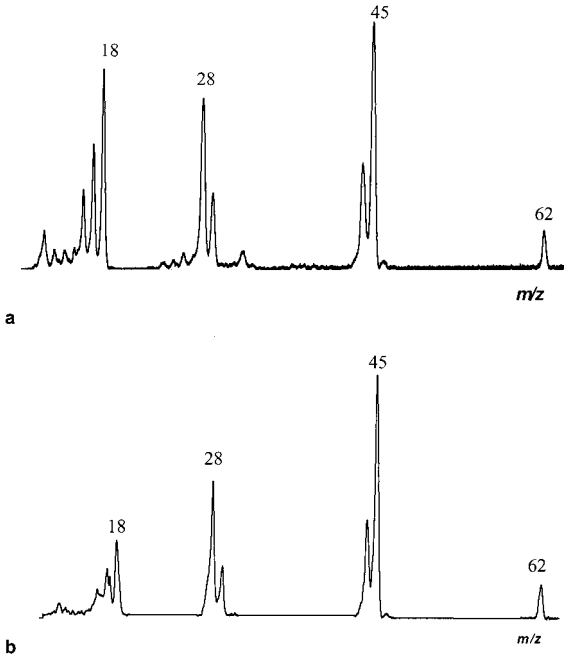

Figure 6. Neutralization (CH_3SSCH_3, 70%T)/reionization (O_2, 70%T) mass spectra of $C(OH)_3^+$ cations (*m*/*z* 63) generated by (a) 70-eV dissociative ionization of di-*n*-propyl carbonate, (b) Xe^+ charge exchange dissociative ionization of di-*n*-propyl carbonate.

Generation of $C(OH)_3$ Radicals. Collisional neutralization of $\mathbf{1}^+$ and $\mathbf{1a}^+$−$\mathbf{1c}^+$ was studied with dimethyl disulfide (Figure 6a) and ammonia (Figure 7a) as electron donors, which gave very similar results. Neutralization with either reagent gave NRMS spectra that did not show any detectable recovery signal at *m*/*z* 63. The major fragments in the NR mass spectra were H_2CO_3 (loss of H), COOH (loss of H_2O or H + OH), CO_2 (loss of H + H_2O), COH, CO, H_2O, OH, and O, at *m*/*z* 62, 45, 44,

TABLE 3: Thermochemical Properties of Carbonic Acid

		energy[a]			
reaction	T (K)	G2(MP2)	G2	QCISD(T)[b]	CCSD(T)[c]
syn-**12** → (^{3}P)C +	0	2491	2489		
3(^{3}P)O + 2(^{2}S)H	298	2523	2521		
$\Delta H^\circ_{f,298}$	0	−607	−605		
	298	−623	−621		
syn-**12** → $CO_2 + H_2O$	0	−34	*d*	−33	−28
	298	−27		−26	−21
$\Delta H^\circ_{f,298}$	298	−608		−610	−614

[a] In units of kJ mol^{-1}. [b] Calculations with the 6-311+G(3df,2p) basis set. [c] Calculations with the aug-cc-pVTZ basis set. [d] G2 calculations give an erroneous energy for CO_2.[33]

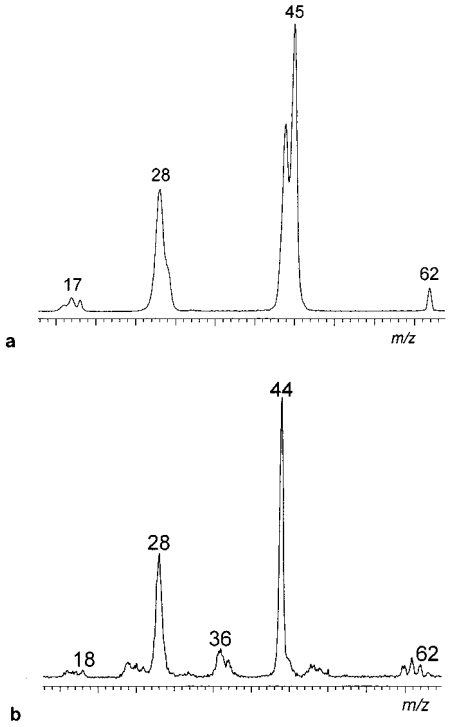

Figure 7. Neutralization (NH_3, 70%T)/reionization (O_2, 70%T) mass spectra of (a) **1**, and (b) **2**.

29, 28, 18, 17, and 16, respectively (Figure 6a). The relative intensities of the NRMS fragment peaks are very similar to those in the previously reported CID spectrum of carbonic acid.[2] This indicates that **1** formed by collisional neutralization dissociates rapidly by loss of a hydrogen atom to form carbonic acid as a stable intermediate. Variable-time measurements were carried out to study the temporal dependence of the NR spectra of $\mathbf{1}^+$. However, even at the shortest flight time of **1** (360 ns) no survivor ion was detected in the NR mass spectrum.

The NRMS spectrum of $\mathbf{1}^+$ prepared by CE ionization with Xe also showed no recovery ion (Figure 6b). The major difference in the NR mass spectra in Figure 6a and 6b was the decreased relative intensity of the $H_2O^{+\bullet}$ peak at m/z 18 in the latter spectrum. This can be readily explained by less efficient collision-induced dissociation, which occurs collaterally with collisional neutralization, of the less energetic ion $\mathbf{1}^+$ from CE ionization. Note that loss of water is the by far most abundant dissociation of $\mathbf{1}^+$, and neutral water is transmitted for reionization together with the products of collisional neutralization. We conclude from the foregoing experiments that the absence of recovery ion is caused by the low stability of **1** when generated by fast electron transfer.

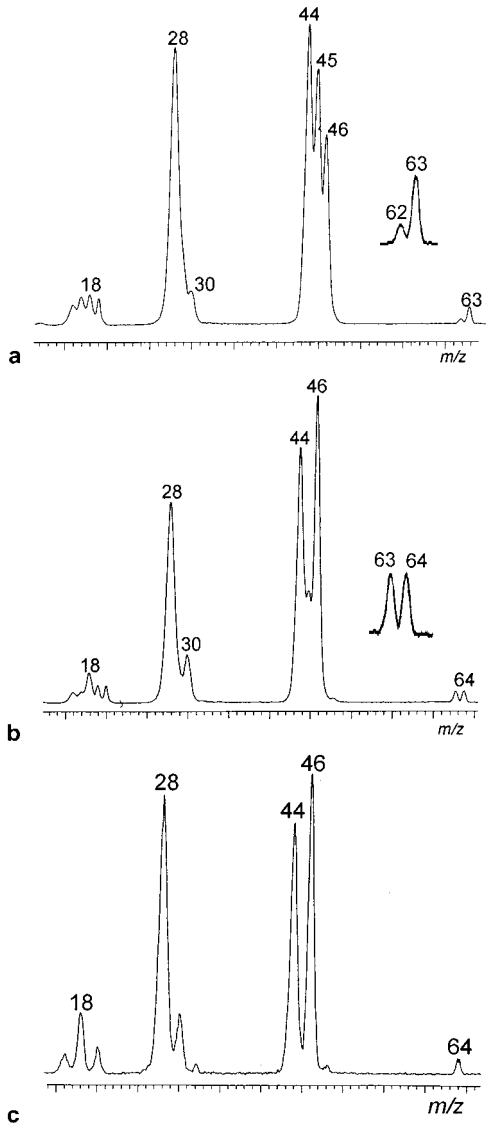

Figure 8. NRMS spectra (NH_3/O_2) of (a) $C(OD)(OH)_2^+$ (m/z 64), (b) $C(OD)_2(OH)^+$ (m/z 65), and (c) $C(OD)_3^+$ (m/z 66). Insets show the expanded regions for loss of H and D peaks.

NR of the proton-bound complex (ion $\mathbf{2}^+$) also resulted in complete dissociation (Figure 7b). The NR mass spectrum of $\mathbf{2}^+$ showed mainly the peaks of $CO_2^{+\bullet}$ and $CO^{+\bullet}$, in keeping with facile dissociation of the transient [O═C═O···H_3O] radical to CO_2 followed by its reionization and ion dissociations. Note that the complementary $H_3O^\bullet$ is an unstable hypervalent radical[49] that is not expected to be detected in the NR mass spectrum.[50] The low-abundance peaks at m/z 24−26, 36, 37, and 48−50 in Figure 6b are due to a trace of a C_5H_3 impurity in the extremely weak ion beam of $\mathbf{2}^+$.

The kinetic stability of a transient species can be increased by using deuterated ion precursors with the assumption that kinetic isotope effects may slow neutral dissociations so that survivor ions could be observed.[51] Despite the possible intervention of kinetic isotope effects, the NR mass spectra of $\mathbf{1a}^+$−$\mathbf{1c}^+$ displayed no survivor ions (Figure 8a−c), and pointed again to fast dissociations of the transient radicals **1a**−**1c**. However, the NR spectra of $\mathbf{1a}^+$ and $\mathbf{1b}^+$ provided the relative intensities of the carbonic acid isotopomers that were used to gauge intramolecular isotope effects on the competitive losses of H and D from **1a** and **1b**. From the integrated peak intensities we find the ratio [**1a**−H]/[**1a**−D] = 3.47, whereas [**1b**−H]/[**1b**−D] = 0.91. Intramolecular isotope effects have been shown

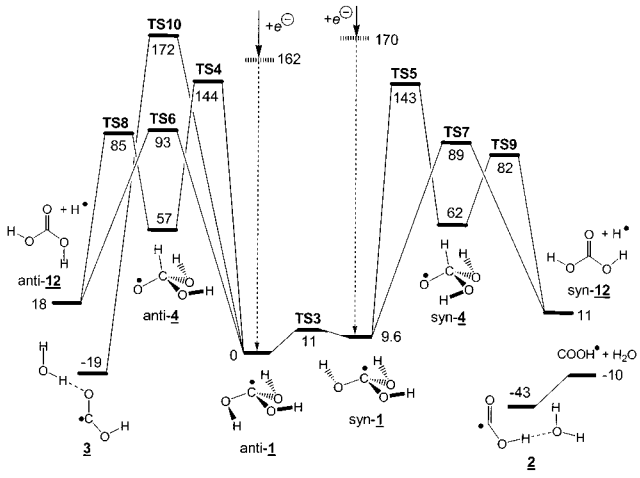

Figure 9. Potential energy diagram for isomerizations and dissociations of $[C,H_3,O_3]$ radicals. 0 K energies from single-point QCISD(T)/6-311+G(3df,2p) calculations.

TABLE 4: Relative Energies of $[C,H_3,O_3]$ Radicals

	relative energy[a]			
species/reaction	G2(MP2)	G2	QCISD(T)[b]	B3-PMP2[b,c]
anti-**1** (C_3)	0	0	0	0
syn-**1** (C_1)	9.4	9.6	9.6	9.7
2	−43	−42	−43	−47
3	−20	−19	−19	−23
anti-**4**	59	58	57	67
syn-**4** (C_s)	65	64	62	71
anti-**1** → syn-**12** + H•	11	11	11	8
anti-**1** → anti-**12** + H•	18	18	18	14
anti-**1** → COOH + H_2O	−12	−10	−10	−16
anti-**1** → (^{1}A)HO—C—OH + OH•	242	243	241	255
anti-**1** → **TS3**	11	11	11	11
anti-**1** → **TS4**	144	143	144	140
syn-**1** → **TS5**	132	132	133	129
anti-**1** → **TS6**	94	93	93	78
syn-**1** → **TS7**	81	80	79	65
anti-**4** → **TS8**	27	27	28	12
syn-**4** → **TS9**	18	18	20	3
anti-**1** → **TS10**	170	171	172	165
anti-**1** → **TS11**	76	77	78	71
syn-**12** → **TS12**	39	39		40

[a] In units of kJ mol^{-1} at 0 K. [b] From single-point calculations with the 6-311+G(3df,2p) basis set. [c] Averaged B3LYP and PMP2 relative energies.

previously to provide valuable information on the amount and distribution of internal energy in transient radicals,[52] as discussed below. To shed more light on the radical energetics and dissociation kinetics, we performed extensive ab initio calculations that are presented and discussed next. The relative and transition state energies referred to in the text and depicted in a potential energy diagram (Figure 9) are from the QCISD(T)/6-311+G(3df,2p) calculations. Relative energies obtained at the other levels of theory are summarized in Table 4.

Radical Structures and Energies. Radical **1** was calculated to exist as two conformers (Figure 10), the more stable anti-**1** of C_3 symmetry, and syn-**1** of C_1 symmetry that was 9.6 kJ mol^{-1} less stable than anti-**1** at 0 K. The greater stability of anti-**1** is consistent with the most favorable orientation of the O—H bond dipoles, as in the ion, anti-$\mathbf{1}^+$. The conformers are separated by a 11 kJ mol^{-1} barrier to OH group rotation (**TS3**, Figure 11) relative to anti-**1**, which allows for very fast conformer interconversion (vide infra). The barrier for OH group rotation in anti-**1** is substantially lower than in the corresponding cation anti-$\mathbf{1}^+$ (vide supra). This results from antibonding

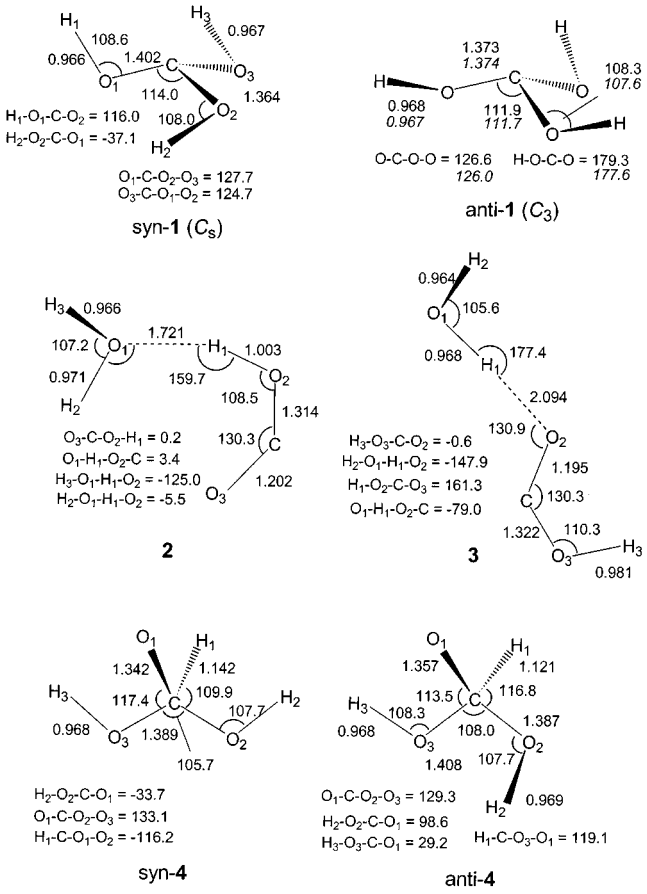

Figure 10. Optimized geometries of $[C,H_3,O_3]$ radicals. Roman numerals, UB3LYP/6-31+G(d,p) geometries. Italics: UMP2(FULL)/6-31+G(d,p) geometries.

π-electron interactions between the C and O atoms in the radical, as also reported previously for analogous systems.[53,54] Four additional $[C,H_3,O_3]$ isomers were found as bound structures by B3LYP and MP2(FULL)/6-31+G(d,p) optimizations. Radicals syn-**4** and anti-**4** (Figure 10) are dihydroxymethoxy rotamers that are 57 and 62 kJ mol^{-1} less stable than anti-**1** (Table 4). In addition, anti-**4** and syn-**4** are separated from anti-**1** and syn-**1**, respectively, by large potential energy barriers for hydrogen atom migration from the O—H groups to the carbon atom (Table 4). The corresponding transition state geometries (**TS4** and **TS5**) are depicted in Figure 11. The most stable $[C,H_3,O_3]$ radical isomer is an $H_2O\cdots HOOC^\bullet$ complex (**2**, Figure 9) in which the oxygen atom of the water molecule is hydrogen bonded to the proton of the COOH radical. Radical **2** is 43 kJ mol^{-1} more stable than anti-**1**. Finally, we found another hydrogen-bonded complex (**3**, Figure 9), in which one of the water protons binds to the carbonyl oxygen of the COOH radical, and which was 19 kJ mol^{-1} more stable than anti-**1**.

Radicals anti-**1** and syn-**1** are kinetically stable against dissociation. Loss of a hydrogen atom from anti-**1** produces the less stable anti-conformer of carbonic acid (anti-**12**), and this dissociation requires only 18 kJ mol^{-1} at the 0 K thermochemical threshold. However, the O—H bond cleavage must overcome a substantial potential energy barrier in the transition state (**TS6**), which is 93 kJ mol^{-1} above anti-**1** (Figure 9). Dissociation of the syn-**1** rotamer proceeds through a different transition state (**TS7**), which is 79 kJ mol^{-1} above syn-**1** and yields the more stable rotamer of carbonic acid, syn-**12**.

Alternative pathways for hydrogen atom loss from anti,syn-**1** are endothermic isomerizations to anti,syn-**4** followed by dissociation of the C—H bonds. However, Figure 9 shows that

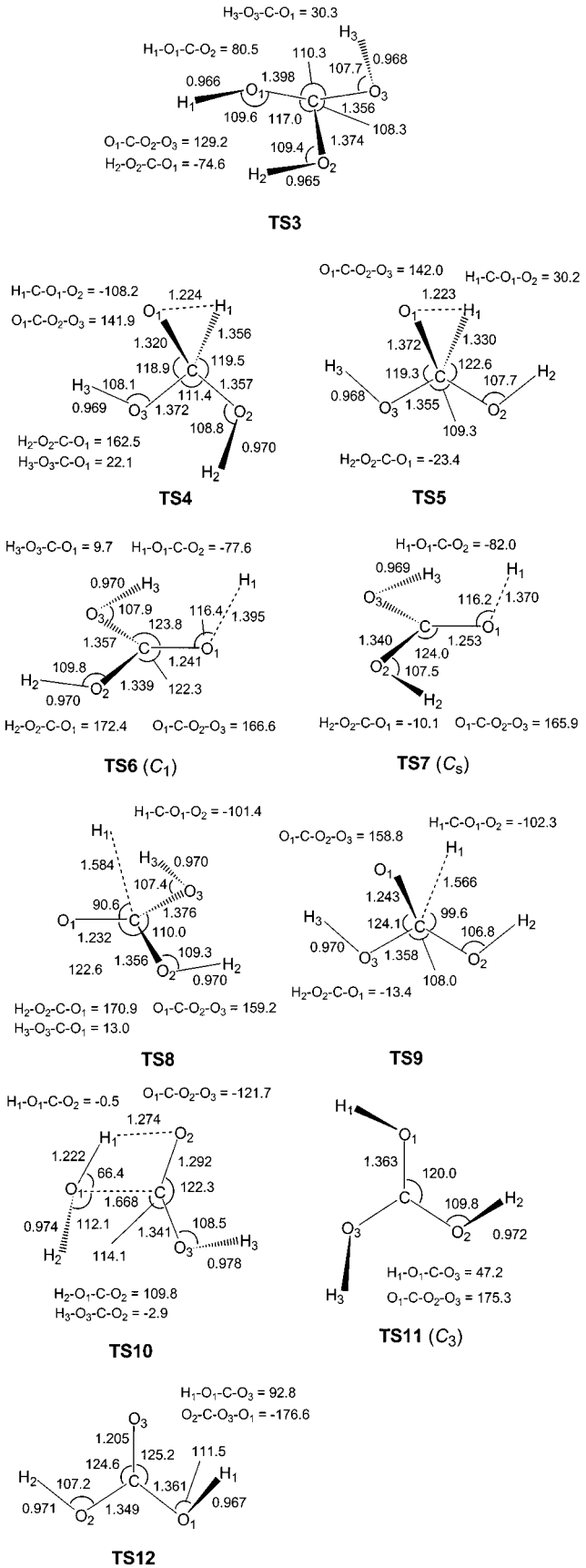

Figure 11. UB3LYP/6-31+G(d,p) optimized transition state geometries.

either isomerization step requires a substantial energy in the transition state (e.g., 144 kJ mol^{-1} from anti-**1** to **TS4**), which should hamper the loss of hydrogen by the two-step mechanism.

Elimination of water from anti-**1** and syn-**1** has the lowest thermochemical threshold which is 10−20 kJ mol^{-1} *below* the respective reactant energies, making the trihydroxymethyl radicals metastable with respect to the exothermic loss of water (Figure 9). However, an elimination of water necessitates a hydrogen migration between the hydroxy groups in anti-**1** which requires 172 kJ mol^{-1} in the transition state (**TS10**, Figure 9) and this high energy disfavors the elimination. It can be concluded from the dissociation energetics that loss of an H atom is the most favorable dissociation of anti-**1** and syn-**1**.

Franck−Condon Effects on Neutralization. The previous discussion showed that loss of H atoms from anti-**1** and syn-**1** should dominate the unimolecular dissociations of the trihydroxymethyl radicals. We now address two questions pertinent to the radical dissociations: (1) What causes the very fast dissociation of radicals anti-**1** and syn-**1** that prevents their detection on a nanosecond time scale in the variable-time NR mass spectra? (2) What is the branching ratio for the formation of the syn and anti rotamers of carbonic acid by loss of H?

A usual cause of excitation in transient species produced by femtosecond collisional electron transfer is the Franck−Condon effects.[55] The internal energy acquired by vertical electron transfer (E_{FC}) is estimated from ab initio calculations by simply adding an electron to the corresponding cation while freezing the molecular geometry. These calculations show that vertical electron capture results in substantial excitation in anti-**1** and syn-**1**, E_{FC} = 162 and 170 kJ mol^{-1}, respectively. The reasons for the large Franck−Condon energies follow from the comparison of the equilibrium geometries of anti- and syn-**1**$^+$ and anti- and syn-**1**,. The major differences in the cation and radical geometries are in the lengths of the C−O bonds which are shorter in the cation (1.285 Å in anti-**1**$^+$ compared to 1.373 Å in anti-**1**), and the O−C−O bond angles which are 120° in the planar cation, but 112° in the pyramidal radical (Figures 3 and 10). Hence, vertical neutralization of anti-**1**$^+$ causes compression of the C−O bonds, resulting in an increased potential energy which is converted to vibrational energy of the radical. The effect of planarization in anti-**1** was investigated by calculating the energy barrier for an umbrella inversion about the carbon atom (**TS11**, Table 4, Figure 11). The calculated E_{TS} = 78 kJ mol^{-1} indicates that the angular distortion in vertically formed planar anti-**1** contributes <50% of the overall Franck−Condon energy. Internal excitation by Franck−Condon effects alone is sufficient to drive dissociations of anti-**1** and syn-**1** because the E_{FC} are greater than the transition state energies (Figure 9).

An obvious consequence of large Franck−Condon effects is the very different vertical and adiabatic ionization energies of the radicals and the recombination energies of the cations. The calculated energies are summarized in Table 2. Adiabatic ionization of anti-**1** and syn-**1** requires 5.82 and 5.98 eV at our highest level of theory. This is substantially lower than the ionization energy of hydroxymethyl radical (7.56 eV),[42,54] and the difference reflects a combination of an increased stabilization of the substituted methyl cation by the π-donating hydroxy groups[47] and destabilization of the radical by the same electronic interaction.[6b,c] Vertical electron capture in anti-**1**$^+$ and syn-**1**$^+$ releases 4.1 eV and results in vibrational excitation in the radicals formed, such that the internal energy exceeds the barriers to dissociation, as discussed above. Vertical ionization of relaxed anti-**1** requires 7.70 eV and forms the cation with ca. 180 kJ mol^{-1} internal energy due to Franck−Condon effects. This is below the threshold for elimination of water from anti-**1**$^+$ (see Table 1), indicating that vertical ionization alone should not lead to extensive dissociation of the ion. The ionization

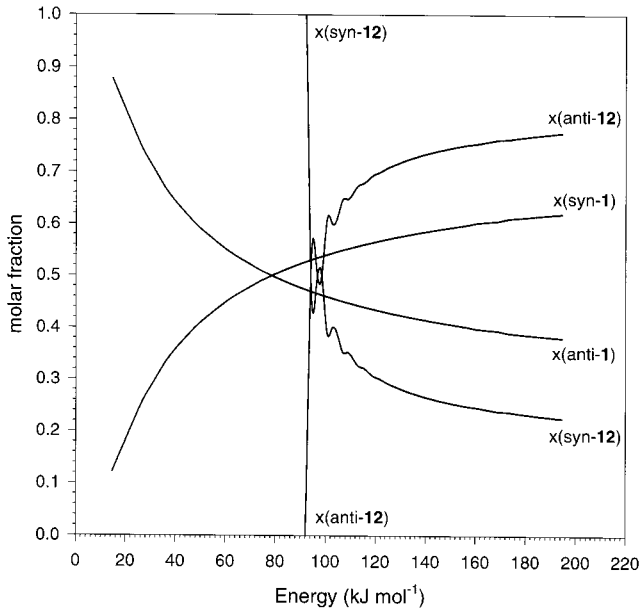

Figure 12. Calculated molar fractions of anti-**1** {*x*(anti-**1**)} and syn-**1** {*x*(syn-**1**)} and the branching ratios for dissociations by H loss forming anti-**12** {*x*(anti-**12**)} and syn-**12** {*x*{syn-**12**)}.

energies further confirm that the absence of a survivor ion in the NR mass spectrum of anti-$\mathbf{1}^+$ is due to radical dissociations.

Radical Dissociation Kinetics. The dissociations on the QCISD(T) potential energy surfaces of anti-**1** and syn-**1** were investigated by RRKM calculations. Because of the very low barrier to interconversion, anti-**1** ↔ syn-**1**, when compared to the dissociation energies, the conformers were considered to equilibrate rapidly at all excitations relevant for dissociation. This was confirmed by the calculated rate constants, k_1 and k_{-1}, for isomerization of anti-**1** to syn-**1** and vice versa, respectively. At internal energies $E > 15$ kJ mol^{-1}, k_1 and k_{-1} exceeded 10^{12} s^{-1}. The energy-dependent molar fractions of anti-**1** and syn-**1** were calculated from the equilibrium constant, $K_{eq}(E) = k_{-1}(E)/k_1(E)$ while taking into account the reaction degeneracies. Because of molecular symmetry, the isomerization anti-**1** → syn-**1** is triply degenerate due to the rotation of any of three O−H bonds to reach the transition state.[48] By the same reasoning, the reverse isomerization, syn-**1** → anti-**1** is doubly degenerate, because the transition state can be achieved by two different rotations of the O−H bonds. This degeneracy entropically favors syn-**1** and gradually compensates the small difference in the conformer relative energies, so that at $E \geq 78$ kJ mol^{-1}, syn-**1** is favored and the molar fraction ratio, x_{syn}/x_{anti}, approaches the statistical 3:2 limit at high internal energies (Figure 12). The conformer population further affects the branching ratio for dissociations by loss of H, whereby anti-**1** dissociates to form anti-**12**, while syn-**1** forms syn-**12**. These bond dissociations are also affected by reaction path degeneracies that differ for anti-**1** and syn-**1**. The cleavage of the out-of-plane O−H bond in syn-**1** has the lowest transition state energy and so the formation of syn-**12** dominates in the narrow interval of internal energies between **TS7** and **TS6** (89−93 kJ mol^{-1}, Figure 9). Note that only a single O−H bond can dissociate in syn-**1** to produce syn-**12** through **TS7**. In contrast, O−H bond dissociation in anti-**1** is triply degenerate, because dissociation of any O−H bond forms anti-**12** through **TS6**. To compare the rate constants for the formation of syn-**12** and anti-**12**, the unimolecular dissociation rate constants, $k_{syn}(E)$ and $k_{anti}(E)$ must be adjusted for the reaction path degeneracy and

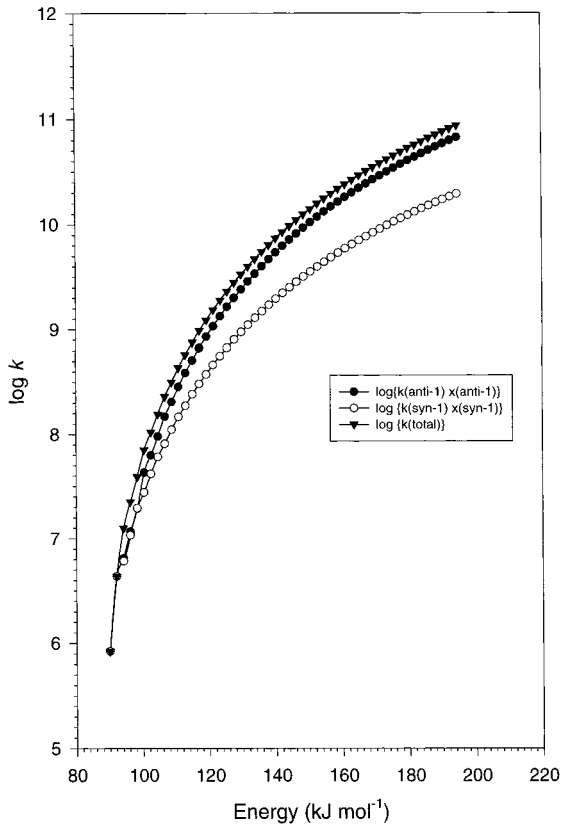

Figure 13. Population weighted rate constants for loss of H from anti-**1**, log[k(anti-**1**) × x(anti-**1**)] (full circles), syn-**1**, log[k(syn-**1**) × x(syn-**1**)] (empty circles), and the total rate constant, log [k(anti-**1**) × x(anti-**1**) + k(syn-**1**) × x(syn-**1**)], full triangles.

weighted by the conformer populations at given internal energy. These adjusted rate constants (log k) are plotted in Figure 13 together with the overall rate constant for hydrogen loss, $k_{total} = x_{syn}k_{syn} + 3x_{anti}k_{anti}$. The rate constants show that both anti-**1** and syn-**1** dissociate rapidly at energies within a few kJ mol^{-1} above the corresponding transition state. At excitation energies gained by Franck−Condon effects (162−170 kJ mol^{-1}, Figure 9), the rate constants approach 10^{10} s^{-1}, so that no surviving radicals can be expected after 360 ns, which was the shortest observation time in the variable NR measurements (vide supra). Experiment and theory are thus in accord in accounting for the complete dissociation of the anti and syn conformers of **1**.

The energy-dependent formation of syn-**12** and anti-**12** is depicted in Figure 12. The branching ratios of molar fractions for syn-**12** and anti-**12** oscillate at low excitation energies due to the effects of limited quantum state densities near the transition state energies that cause oscillations in the unimolecular rate constants. Despite the lower TS energy for the dissociation of syn-**1**, the dissociation of anti-**1** is favored by entropy effects due to the reaction path degeneracy, so that anti-**1** dissociates faster at $E \geq 98$ kJ mol^{-1} (Figure 12). Formation of the less stable anti-**12** is thus kinetically favored at higher excitation energies.

To make the situation even more complicated, once formed, syn-**12** and anti-**12** can isomerize unimolecularly by O−H bond rotations. The rotation barrier (**TS12**, 39 kJ mol^{-1} above syn-**12**) is readily overcome in syn- and anti-**12** produced by dissociations of syn- and anti-**1**, respectively. From the energy excess in the dissociating radicals, e.g. $E_{exc} = E_{FC} - \Delta H_{rxn,0} =$ 162−18 = 144 kJ mol^{-1} for anti-**1**, it follows that the carbonic acid formed must have a substantial internal energy. A fraction

of the energy excess can go into the translational recoil energy of H and anti-**12**. Nevertheless, RRKM calculations show that, for $E \geq 75$ kJ mol^{-1}, the rate constants of interconversion are $>10^{11}$ s^{-1}, so that the carbonic acid conformers rapidly reach equilibrium populations that approach the statistical 2:1 ratio, e.g., 64% anti-**12** and 36% syn-**12** at 144 kJ mol^{-1} of internal energy.

Before continuing to the analysis of isotope effects, it is useful to summarize the dissociation kinetics of radicals **1**. Anti and syn-**1** rapidly interconvert by O−H bond rotations through **TS3**, so that dissociating radicals reach equilibrium populations of conformers in which syn-**1** is more abundant. At internal energies >100 kJ mol^{-1}, anti-**1** dissociates faster than syn-**1** to form anti-**12**. Due to the energy excess imparted in syn-**1** and anti-**1** by Franck−Condon effects, the anti-**12** and syn-**12** formed by dissociation further equilibrate by O−H bond rotations through **TS12** to finally establish a 2:1 anti:syn ratio of conformers.

Kinetic Isotope Effects and Internal Energy Distribution in Radicals Formed by Electron Transfer. While the unimolecular dissociations of radical **1** are too fast to be measured by variable-time NR, the relative rates for losses of H and D are readily available from regular NR mass spectra of **1a** and **1b** (Figure 8). The spectra provide estimates of intramolecular kinetic isotope effects,[56] [H]/[D], from the integrated intensities of the $(\mathbf{1a}-\mathrm{H})^{+\bullet}$ and $(\mathbf{1a}-\mathrm{D})^{+\bullet}$ ions, and likewise for $(\mathbf{1b}-\mathrm{H})^{+\bullet}$ and $(\mathbf{1b}-\mathrm{D})^{+\bullet}$. It is assumed that the carbonic acid isotopomers have very similar ionization cross sections, and that the fractions of surviving $(\mathbf{1a}-\mathrm{H})^{+\bullet}$ and $(\mathbf{1a}-\mathrm{D})^{+\bullet}$ ions are proportional to the populations of the neutral molecules being formed, in other words, that isotope effects on ion dissociations following reionization can be neglected. The experimental isotope effects can be expressed by eq 3,

$$\frac{[\mathrm{H}]}{[\mathrm{D}]} = \frac{\int_0^{\tau} \mathrm{d}t \int_{E_{a,H}}^{\infty} f_H[k_H(E),k_D(E)]P(E)[1 - e^{-(k_H(E)t/\Sigma k(E))}]\,\mathrm{d}E}{\int_0^{\tau} \mathrm{d}t \int_{E_{a,D}}^{\infty} f_D[k_H(E),k_D(E)]P(E)[1 - e^{-(k_D(E)t/\Sigma k(E))}]\,\mathrm{d}E} \quad (3)$$

where $k_H(E)$ and $k_D(E)$ are the unimolecular rate constants from RRKM calculations, E is the radical internal energy, $P(E)$ is the internal energy distribution function, $E_{a,H}$ and $E_{a,D}$ are the transition state energies for loss of H and D, respectively, and τ is the time for dissociation. Because the dissociations are very fast, so that $k(E)\tau \gg 1$, eq 3 is simplified to eq 4, where $f[k_H(E), k_D(E)]$ are combinations of unimolecular rate constants for loss of H and D depending on the system in question.

$$\frac{[\mathrm{H}]}{[\mathrm{D}]} = \frac{\int_{E_{a,H}}^{\infty} f_H[k_H(E),k_D(E)]P(E)\,\mathrm{d}E}{\int_{E_{a,D}}^{\infty} f_D[k_H(E),k_D(E)]P(E)\,\mathrm{d}E} \quad (4)$$

Functions $f[k_H(E),k_D(E)]$ are shown in Scheme 3 for dissociations of syn- and anti-**1a**, and analogous functions were derived for dissociations of syn- and anti-**1b** in which the subscripts for H and D were reversed. Note that the presence of deuterium disrupts molecular symmetry, so that a rigorous treatment requires that separate reactants and transition states be used to evaluate $k_H(E)$ and $k_D(E)$ in the conformers, as well as the energy-dependent conformer molar fractions x_{anti} and x_{syn}. In calculations of molar fractions, kinetic isotope effects on O−H bond rotation can be neglected at internal energies at or above **TS6** and **TS7**, and so the three isotopomers of syn-**1a** and syn-**1b** were treated as identical molecules.

SCHEME 3

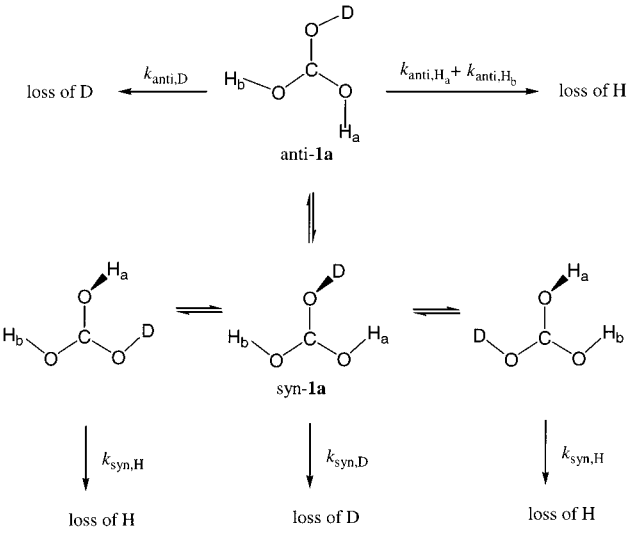

$$f_H[k_H(E), k_D(E)] = \frac{x_{anti}[k_{anti,H_a} + k_{anti,H_b}] + 2x_{syn}k_{syn,H}}{x_{anti}[k_{anti,H_a} + k_{anti,H_b}] + 2x_{syn}k_{syn,H} + x_{syn}k_{syn,D}}$$

$$f_D[k_H(E), k_D(E)] = \frac{x_{anti}k_{anti,D} + x_{syn}k_{syn,D}}{x_{anti}[k_{anti,H_a} + k_{anti,H_b}] + 2x_{syn}k_{syn,H} + x_{syn}k_{syn,D}}$$

The internal energy distribution function $P(E)$ was modeled as a two-parameter, normalized, Boltzmann-like function (eq 5),[51] where E_0 is an onset energy and W is a width parameter. Function $P(E)$ shows a maximum at $E_{max} = E_0 + W/2$ and gives the population mean

$$P(E) = \frac{4(E - E_0)}{W^2} e^{-(2(E-E_0)/W)} \quad (5)$$

at $\langle E \rangle = E_0 + W$. The E_{max} and $\langle E \rangle$ represent the most probable and mean internal energy in the transient neutral species produced by vertical neutralization. Parameters E_0 and W were least-squares fitted in eq 4 to obtain the best agreement with the experimental isotope effects for loss of H and D from **1a** and **1b**. The best fit was obtained for $E_0 = 110$ kJ mol^{-1} and $W = 138$ kJ mol^{-1}, which gave [H]/[D] = 3.48 for **1a** to be compared with the experimental value of 3.47, and [H]/[D] = 0.89 for **1b** to be compared with 0.91 from experiment. These parameters set the most probable internal energy in **1a,b** at $E_{max} = 110 + 138/2 = 179$ kJ mol^{-1}. Presuming virtually the same internal energy distribution in the nonlabeled radicals anti-**1** and syn-**1**, the potential energy diagram in Figure 9 shows that, out of the overall vibrational excitation, 162 kJ mol^{-1} originates from Franck−Condon effects on vertical neutralization, so the remaining 17 kJ mol^{-1} must originate from the internal energy of the precursor ion, which is most likely the more stable anti-$\mathbf{1}^+$. Such a small amount of internal energy in the precursor ion appears reasonable. Anti-$\mathbf{1}^+$ is formed from di-*n*-alkyl carbonate precursors by a rearrangement that requires three hydrogen migrations; such a rearrangement can compete with α-cleavage dissociations of the C−O bonds at ion energies close to the dissociation threshold, implying low excitation in the products. It is interesting to note that the most probable internal energy calculated for anti-**1** is very close to a simple sum of the Franck−Condon energy from vertical neutralization and the

thermal energy of the precursor ion at the ion source temperature (vide supra), $162 + 20 = 182$ kJ mol^{-1}. This leads to the conclusion that the principal mechanism of internal energy transfer in femtosecond electron transfer is through Franck−Condon effects, whereas other mechanisms, such as collisional activation, are secondary or negligible.

Conclusions

This combined experimental and computational study allows us to make several conclusions. Trihydroxymethyl radicals syn- and anti-**1** are intrinsically stable species in an isolated state. Upon formation by femtosecond electron transfer to trihydroxymethyl cations, the radicals gain internal energies that are sufficient to cause rapid dissociation by loss of hydrogen atoms. Analysis of the isotope effects on the hydrogen and deuterium atom losses indicates that the radicals have internal energies that can be expressed as a simple sum of the cationic precursor energy and the Franck−Condon energy acquired by vertical electron transfer.

Acknowledgment. Support of this work by the National Science Foundation (Grant CHE-0090930) is gratefully acknowledged. Computational support was provided jointly by the NSF-CRIF Program (Grant CH-9808182) and the University of Washington. We thank Dr. Martin Sadílek for technical assistance with spectra measurements and Professor Robert Flammang of the University of Mons-Hainaut for his interest and support.

References and Notes

(1) (a) Galinos, A. G.; Carotti, A. A. *J. Am. Chem. Soc.* **1961**, *83*, 752. (b) Gattow, G.; Gewarth, U. *Angew. Chem., Int. Ed. Engl.* **1965**, *4*, 149.

(2) Terlouw, J. K.; Lebrilla, C. B.; Schwarz, H. *Angew. Chem., Int. Ed. Engl.* **1987**, *26*, 354−355.

(3) (a) Olah, G. A.; White, M. *J. Am. Chem. Soc.* **1968**, *90*, 1884−1889. (b) Rasul, G.; Reddy, V. P.; Zdunek, L.; Prakash, G. K. S.; Olah, G. A. *J. Am. Chem. Soc*. **1993**, *115*, 2236−2238.

(4) Egsgaard, H.; Carlsen, L. *J. Chem. Soc., Faraday Trans. 1* **1989**, *85*, 3403−3411.

(5) (a) Lazarou, Y. G.; Papagiannakopoulos, P. *J. Phys. Chem.* **1993**, *97*, 9133−9140. (b) Burkey, T. J.; Castelhano, A. L.; Griller, D.; Lossing, F. P. *J. Am. Chem. Soc*. **1983**, *105*, 4701−4703.

(6) For comprehensive computational studies see: (a) Pasto, D. J. *J. Am. Chem. Soc.* **1988**, *110*, 8164−8175. (b) Leroy, G.; Sana, M.; Wilante, C. *THEOCHEM* **1991**, *74*, 37−45. (c) Leroy, G.; Sana, M.; Wilante, C. *THEOCHEM* **1991**, *80*, 303−328. (d) Pius, K.; Jain, M.; Chandrasekhar, J. *THEOCHEM* **1996**, *361*, 191−203. (e) Wayner, D. D. M.; Clark, K. B.; Rauk, A. Yu. D.; Armstrong, D. A. *J. Am.* Chem. Soc. **1997**, *119*, 8925−8932. (f) Mayer, P. M.; Glukhovtesev, M. N.; Gauld, J. W.; Radom, L. *J. Am. Chem. Soc.* **1997**, *119*, 12889−12895. (g) Parkinson, C. J.; Mayer, P. M.; Radom, L. *J. Chem. Soc., Perkin Trans. 2* **1999**, 2305−2313. (h) Henry, D. J.; Parkinson, C. J.; Mayer, P. M.; Radom, L. *J. Phys. Chem. A* **2001**, *105*, 6750−6756.

(7) Finlayson-Pitts, B. J. *Chemistry of the Upper and Lower Atmosphere: Theory, Experiments, and Applications*; Academic Press: San Diego, 2000.

(8) For pyrolytic studies see, for example: (a) Werstiuk, N. H. *Can. J. Chem.* **1986**, *64*, 2175−2183. (b) Sendt, K.; Ikeda, E.; Bacskay, G. B.; Mackie, J. C. *J. Phys.* Chem. A **1999**, *103*, 1054−1072.

(9) For photochemical studies of substituted methyl radicals see, for example: (a) Hudgens, J. W.; Johnson, R. D., III; Tsai, B. P. *J. Chem. Phys.* **1993**, *98*, 1925−1932. (b) Cyr, D. R.; Leahy, D. J.; Osborn, D. L.; Continetti, R. E.; Neumark, D. M. *J. Chem. Phys.* **1993**, *99*, 8751−8764. (c) Yang, X.; Felder, P.; Huber, J. R. *Chem. Phys.* **1994**, *189*, 127−136. (d) Reed, C. L.; Kono, M.; Ashfold, M. N. R. *J. Chem. Soc., Faraday Trans.* **1996**, *92*, 4897−4904. (e) Ashfold, M. N. R.; Dixon, R. N.; Kono, M.; Mordaunt, D. H.; Reed, C. L. *Philos. Trans. R. Soc. London, Ser. A* **1997**, *355*, 1659−1676. (f) Moriyama, M.; Tsutsui, Y.; Honma, K. *J. Chem. Phys.* **1998**, *108*, 6215−6221. (g) Conroy, D.; Aristov, V.; Feng, L.; Reisler, H. *J. Phys. Chem. A* **2000**, *104*, 10288−10292.

(10) For H atom abstraction studies see: (a) Jacox, M. E. *J. Phys. Chem.* **1983**, *87*, 3126−3135. (b) Kuo, S.-C.; Zhang, Z.; Klemm, R. B.; Liebman, J. F.; Stief, L. J.; Nesbitt, F. L. *J. Phys. Chem.* **1994**, *98*, 4026−4033. (c) Baker, J.; Dyke, J. M.; Ellis, A. R.; Morris, A. *J. Electron Spectrosc. Relat. Phenom.* **1995**, *73*, 125−138. (d) Dobe, S.; Berces, T.; Turanyi, T.; Marta, F.; Grussdorf, J.; Temps, F.; Wagner, H. G. *J. Phys. Chem.* **1996**, *100*, 19864−19873. (e) Tyndall, G. S.; Orlando, J. J.; Kegley-Owen, C. S.; Wallington, T. J.; Hurley, M. D. *Int. J. Chem. Kinet.* **1999**, *31*, 776−784. (f) Jansen, T. C.; Trabjerg, I.; Rettrup, S.; Pagsberg, P.; Sillesen, A. *Acta Chem. Scand.* **1999**, *53*, 1054−1058. (g) Wang, B.; Hou, H.; Gu, Y. *J. Phys. Chem. A* **2001**, *105*, 156−164.

(11) For comprehensive reviews of the technique see: (a) Wesdemiotis, C.; McLafferty, F. W. *Chem. Rev.* **1987**, *87*, 485−500. (b) Holmes, J. L. *Mass Spectrom.* Rev. **1989**, *8*, 513−539. (c) Tureèek, F. *Org. Mass Spectrom.* **1992**, *27*, 1087−1097. (d) Schalley, C. A.; Hornung, G.; Schroder, D.; Schwarz, H. *Chem. Soc. Rev.* **1998**, *27*, 91−104. (e) Zagorevskii, D. V.; Holmes, J. L. *Mass Spectrom. Rev.* **1999**, *18*, 87−118.

(12) Harnish, D.; Holmes, J. L. *Org. Mass Spectrom.* **1994**, *29*, 213−219.

(13) Harvey, J. N.; Schroder, D.; Schwarz, H. *Bull. Soc. Chim. Belg.* **1997**, *106*, 447−453.

(14) Shaffer, S. A.; Tureček, F.; Cerny, R. L. *J. Am. Chem. Soc*. **1993**, *115*, 12117−12124.

(15) Polášek, M.; Tureček, F. *J. Phys. Chem. A* **2001**, *105*, 1371−1382.

(16) Wiedmann, F. A.; Wesdemiotis, C. *J. Am. Chem. Soc.* **1994**, *116*, 2481−2485.

(17) Sadílek, M.; Tureček, F. *J. Phys. Chem.* **1996**, *100*, 224−232.

(18) Schalley, C. A.; Schroeder, D.; Schwarz, H. *Int. J. Mass Spectrom. Ion Processes* **1996**, *153*, 173−199.

(19) Syrstad, E. A.; Tureček, F. *J. Phys. Chem. A* **2001**, *105*, 11144−11155.

(20) Larock, R. C.; Lee, N. H. *Tetrahedron Lett.* **1991**, *32*, 6315−6318.

(21) Cotarca, L.; Delogu, P.; Nardelli, A.; Sunjic, V. *Synthesis* **1996**, 553−576.

(22) Tureček, F.; Gu, M.; Shaffer, S. A. *J. Am. Soc. Mass Spectrom*. **1992**, *3*, 493−501.

(23) Bateman, R. H.; Brown, J.; Lefevere, M.; Flammang, R.; Van Haverbeke, Y. *Int. J. Mass Spectrom. Ion Processes* **1992**, *115*, 205−218.

(24) (a) Kuhns, D. W.; Tran, T. B.; Shaffer, S. A.; Tureček, F. *J. Phys. Chem.* **1994**, *98*, 4845−4853. (b) Kuhns, D. W.; Tureèek, F. *Org. Mass Spectrom.* **1994**, *29*, 463−469.

(25) Frisch, M. J.; Trucks, G. W.; Schlegel, H. B.; Scuseria, G. E.; Robb, M. A.; Cheeseman, J. R.; Zakrzewski, V. G.; Montgomery, J. A.; Stratmann, R. E.; Burant, J. C.; Dapprich, S.; Millam, J. M.; Daniels, A. D.; Kudin, K. N.; Strain, M. C.; Farkas, O.; Tomasi, J.; Barone, V.; Cossi, M.; Cammi, R.; Mennucci, B.; Pomelli, C.; Adamo, C.; Clifford, S.; Ochterski, J.; Petersson, G. A.; Ayala, P. Y.; Cui, Q.; Morokuma, K.; Malick, D. K.; Rabuck, A. D.; Raghavachari, K.; Foresman, J. B.; Cioslowski, J.; Ortiz, J. V.; Stefanov, B. B.; Liu, G.; Liashenko, A.; Piskorz, P.; Komaromi, I.; Gomperts, R.; Martin, R. L.; Fox, D. J.; Keith, T.; Al-Laham, M. A.; Peng, C. Y.; Nanayakkara, A.; Gonzalez, C.; Challacombe, M.; Gill, P. M. W.; Johnson, B. G.; Chen, W.; Wong, M. W.; Andres, J. L.; Head-Gordon, M.; Replogle, E. S.; Pople, J. A. *Gaussian 98*, Revision A.6; Gaussian, Inc.: Pittsburgh, PA, 1998.

(26) (a) Becke, A. D. *J. Chem. Phys.* **1993**, *98*, 1372−1377. (b) Becke, A. D. *J. Chem. Phys.* **1993**, *98*, 5648−5652. (c) Stephens, P. J.; Devlin, F. J.; Chabalowski, C. F.; Frisch, M. J. *J. Phys. Chem.* **1994**, *98*, 11623−11627.

(27) Møller, C.; Plesset, M. S. *Phys. Rev.* **1934**, *46*, 618−622.

(28) (a) Mayer, I. *Adv. Quantum Chem.* **1980**, *12*, 189−262. (b) Schlegel, H. B. *J. Chem.* Phys. **1986**, *84*, 4530−4534.

(29) Rahut, G.; Pulay, P. *J. Phys. Chem.* **1995**, *99*, 3093−3100.

(30) Curtiss, L. A.; Raghavachari, K.; Pople, J. A. *J. Chem. Phys.* **1993**, *98*, 1293−1298.

(31) Curtiss, L. A.; Raghavachari, K.; Trucks, G. W.; Pople, J. A. *J. Chem. Phys.* **1991**, *94*, 7221−7230.

(32) Pople, J. A.; Head-Gordon, M.; Raghavachari, K. *J. Chem. Phys.* **1987**, *87*, 5968−5975.

(33) Nicolaides, A.; Radom, L. *J. Phys. Chem.* **1994**, *98*, 3092−3093.

(34) Čížek, J.; Paldus, J.; Šroubková, L. *Int. J. Quantum Chem.* **1969**, *3*, 149−167.

(35) Purvis, G. D.; Bartlett, R. J. *J. Chem. Phys.* **1982**, *76*, 1910−1918.

(36) Dunning, T. H., Jr. *J. Chem. Phys.* **1989**, *90*, 1007−1023.

(37) Tureček, F. *J. Phys. Chem. A* **1998**, *102*, 4703−4713.

(38) Foresman, J. B.; Head-Gordon, M.; Pople, J. A.; Frisch, M. J. *J. Phys. Chem.* **1992**, *96*, 135−149.

(39) Stratmann, R. E.; Scuseria, G. E.; Frisch, M. J. *J. Chem. Phys.* **1998**, *109*, 8218−8224.

(40) Zhu, L.; Hase, W. L. *Quantum Chemistry Program Exchange*; Indiana University: Bloomington, IN, 1994; Program No. QCPE 644.

(41) Frank, A. J.; Sadílek, M.; Ferrier, J. G.; Tureček, F. *J. Am. Chem. Soc.* **1997**, *119*, 12343−12353.

(42) *NIST Standard Reference Database No. 69*, February 2000 Release. http://webbook.nist.gov.
(43) Brown, P.; Djerassi, C. *J. Am. Chem. Soc.* **1966**, *88*, 2469−2478.
(44) Hrusak, J.; McGibbon, G. A.; Schwarz, H.; Terlouw, J. K. *Int. J. Mass Spectrom. Ion Processes* **1997**, *160*, 117−135.
(45) We thank a reviewer for pointing this out.
(46) Holmes, J. L.; Osborne, A. D. *Org. Mass Spectrom.* **1981**, *16*, 236.
(47) Holmes, J. L.; Lossing, F. P. *Can. J. Chem.* **1982**, *60*, 2365−2371.
(48) Murrell, J. N.; Laidler, K. J. *Trans. Faraday Soc*. **1968**, *64*, 371−377.
(49) Chen, F. W.; Davidson, E. R. *J. Phys. Chem. A* **2001**, *105*, 10915−10921.
(50) Gellene, G. I.; Porter, R. F. *J. Chem. Phys.* **1984**, *81*, 5570−5576.
(51) Nguyen, V. Q.; Shaffer, S. A.; Tureček, F.; Hop, C. E. C. A. *J. Phys. Chem.* **1995**, *99*, 15454−15464.
(52) (a) Wolken, J. K.; Tureček, F. *J. Am. Chem. Soc.* **1999**, *121*, 6010−6018. (b) Wolken, J. K.; Tureček, F. *J. Phys. Chem. A* **1999**, *103*, 6268−6281.
(53) Johnson, R. D., III; Hudgens, J. W. *J. Phys. Chem.* **1996**, *100*, 19874−19890.
(54) Syrstad, E. A.; Tureček, F. *J. Phys. Chem A* **2001**, *105*, 11144−11155.
(55) Nguyen, V. Q.; Tureček, F. *J. Mass Spectrom.* **1996**, *31*, 843−854.
(56) Derrick, P. J. *Mass Spectrom. Rev.* **1983**, *2*, 285−298.